

# Study of the permittivity, permeability and microwave attenuation of zinc ferrites nanoparticles prepared by sol-gel methods

Sabah Ibrahim Abbas <sup>1\*</sup>, Abbas Salam Khamas <sup>2</sup>

<sup>1</sup> Al-Karkh University of science, College of science, Medical physics department, Baghdad, Iraq

<sup>2</sup> University of Wasit, College of Science, Department of Physics, Iraq

\*Corresponding author E-mail: [sabahibab@gmail.com](mailto:sabahibab@gmail.com)

## Abstract

Zinc ferrite nanoparticles is synthesized by the sol-gel method from  $Zn(NO_3)_2 \cdot 6H_2O$  and  $Fe(NO_3)_3 \cdot 9H_2O$  by using molar concentrations (0.2M and 0.4M), and all samples were sintered at temperatures (600 °C, 800°C and 1000°C) for two hours. X-ray diffraction patterns reveal the presence nanoparticles of cubic spinel phase of zinc ferrite structure with a mix of other phases are a hexagonal hematite type of  $\alpha-Fe_2O_3$  and the hexagonal wurtzite structure of ZnO. Morphology characteristic has been examined by using the scanning Probe Microscope and shown the grain size is increasing when the molar concentration increases probably due to the large radius of zinc ions than  $Fe^{3+}$ . Complex permeability, complex permittivity, and attenuation of zinc ferrite composite are investigated in X-band frequency. The real part of magnetic permeability decreases with increasing frequency because the external field changes rapidly at high frequency and the Magnetic loss is very low due to reduce the eddy current. The real and imaginary parts of the permittivity remains nearly constant and low values with increasing frequency for concentrations 0.2M and 0.4M at sintering temperature 600°C. The constant values for real part of permittivity means there was a dominant one type of polarization. The low values of imaginary part of permittivity may be due to decrease of dipole polarization. The best desired absorbance and attenuation of microwave can be achieved at the low values of the sintering temperature (600°C) for two concentration where the reflectivity of the waves at the minimum value.

**Keywords:** Ferrites; Permittivity; Permeability; Microwave Absorber.

## 1. Introduction

Study of microwave absorption materials has been received much attention in recent years because they used in industrial and military purposes [1]. Microwaves absorption is dependent on the chemical compositions and treatment parameters which can greatly influence on the grain size, complex dielectric permittivity ( $\epsilon_r$ ) and complex magnetic permeability ( $\mu_r$ ) [2], [3]. Cubic structure of the Spinal ferrite are described by the form  $(A^{2+})[B^{3+}]_2O_4$ , where (A) is represent the tetrahedral cation site which are occupied by divalent ions and [B] is octahedral cation site which are occupied by trivalent ions) in a Fcc anion oxygen sublattice.  $ZnFe_2O_4$  is a typical example of normal spinal ferrites where  $Fe^{3+}$  ions in the B-cation sites and  $Zn^{2+}$  ions in the A-cation sites [4]. A unit cell consist 32 O-atoms in a cube close packing and 8 Td tetrahedral with 16 Oh octahedral occupied sites [5]. Nano magnetic materials are very important in the applications of high density information storage media and absorption of electromagnetic waves [6]. Ferrites nanoparticles can be manipulated by applying magnetic field, nanoparticles ferrites are important because of their unique magnetic, dielectric electronics, electric, optical, mechanics and catalytic properties [7]. Mixed Metal-Zinc ferrites are characterized by good magnetic properties as high for  $CoFe_2O_4$  low for  $NiFe_2O_4$ , high electrical resistivity, magnetic coercivity and negligible eddy current loss for high frequency electromagnetic fields propagation [8,9]. High resistivity of ferrites materials used for application of moderate frequency in the

range (0.1-1 MHz)[10]. Permittivity and permeability properties show significant dependences on the frequency which causes to higher losses at radio frequencies and ferromagnetic resonance [10]. There are many different methods for preparing  $ZnFe_2O_4$  nanoparticles some of these methods are chemical co-precipitation method [11], hydrothermal synthesis [12], sol-gel method [13], solvothermal synthesis [14], solid-state reaction [15] and thermal plasma synthesis [16]. A. Simona et al [17] have been prepared of  $Zn_xFe_{3-x}O_4$  powder with ( $x = 0.2, 0.5, 0.8, 1, 1.2, 1.5$ ) by a chemical coprecipitation method, and studied the variations of the real and imaginary complex susceptibility parts with frequency. Their results showed that a maximum value for the imaginary part of susceptibility appears at about 3 GHz, where the real part of susceptibility has a minimum. This means that the  $ZnFe_2O_4$  powder presents relatively higher microwave absorbance at 3 GHz. Wang. Jie et al [18] reported the synthesis of  $Mn_{0.8}Zn_{0.2}Fe_2O_4$  ferrite by sol-gel combustion method. They observed that the microwaves absorbing properties are influenced by the weight ratio of ferrite to polymer. They are found the best weight ratio composites of ferrite to polymer being 3:2 have a maximum reflection loss about -16 dB with wide absorbing band. This research depends the sol-gel method to prepare  $ZnFe_2O_4$  nanoparticles and will be investigated the effect of using different molar concentrations (0.2 M, 0.4 M) with equal molar ratios for both  $Fe(NO_3)_3 \cdot 9H_2O$ ,  $Zn(NO_3)_2 \cdot 6H_2O$  to form  $ZnFe_2O_4$  nanoparticles and sintering temperature (600 °C, 800°C and 1000°C) on the

dielectric permittivity and magnetic permeability as well on the microwaves absorption properties.

## 2. Theory

Microwaves are a part of the transverse electromagnetic waves which have the wavelength (1mm-30mm) and frequencies (1-300 GHz). The microwaves frequency consists of many zones of bands and every zone has its special applications, the most important band is X-band (8-12 GHz) because it is widely used in the radar application [19]. The electromagnetic matrix parameters can be derived by the scattering matrix elements and the network analyzer is used to measure the scattering matrix elements ( $S_{11}, S_{12}, S_{21}, S_{22}$ ) [20]. A vector network analyzer can measure two forward waves  $a_1, a_2$  and two reverse waves  $b_1, b_2$ . These elements ( $a_1, a_2, b_1, b_2$ ) can be assumed current or voltage. The matrix scattering parameters (S) which describes the relationships between the output wave (b) and input wave (a) [21].

$$[b] = [S] [a]; [S] = \begin{bmatrix} S_{11} & S_{12} \\ S_{21} & S_{22} \end{bmatrix} \quad (1)$$

$$S_{jj} = \frac{b_j}{a_j} \quad (j = 1, 2); S_{ij} = \frac{b_i}{a_i} \quad (i \neq j; i = 1, 2; j = 1, 2) \quad (2)$$

The reflection coefficient [21]:

$$\Gamma_j = S_{jj} = \frac{b_j}{a_j} \quad (3)$$

The transmission coefficient [21]:

$$T_{j \rightarrow i} = S_{ij} = \frac{b_i}{a_i} \quad (4)$$

The four detectors in the network analyzer system are used to measure the four waves respectively, and the combinations of these four waves in the Eqs. (3) and (4) can be produced the scattering parameters. Nicolson and Ross [22] were derived the formula to measure the dielectric permittivity and magnetic permeability by combined ( $S_{11}$ ) and ( $S_{21}$ ). The reflection coefficient and transmission coefficient are calculated by using the scattering parameters ( $S_{11}$ ) and ( $S_{21}$ ).

$$\Gamma = K \pm \sqrt{K^2 - 1} \quad (5)$$

And

$$K = \frac{(S_{21}^2(\omega) - S_{11}^2(\omega)) + 1}{2S_{11}(\omega)} \quad (6)$$

The transmission coefficient can be described by equation

$$T = \frac{(S_{11}(\omega) + S_{21}(\omega)) - \Gamma}{1 - (S_{11}(\omega) + S_{21}(\omega))\Gamma} \quad (8)$$

Equations (5) and (8), auxiliary variables (x) and (y) are defined as follows equations [23].

$$x = \frac{\mu_r}{\epsilon_r} = \left( \frac{1+\Gamma}{1-\Gamma} \right)^2 \quad (9)$$

$$y = \mu_r \cdot \epsilon_r = \left( \frac{c}{\omega d} \ln \left( \frac{1}{T} \right) \right)^2 \quad (10)$$

$$\mu_r = \sqrt{x \cdot y}; \epsilon_r = \sqrt{\frac{y}{x}} \quad (11)$$

Where  $\mu_r$  is the relative permeability of material;  $\epsilon_r$  is the relative permittivity of material;  $\omega$  is the angular frequency; c is the light speed.

The parameter ( $\Lambda$ ) is given by equation [23]:

$$\frac{1}{\Lambda^2} = \left( \frac{\epsilon_r \mu_r}{\lambda_o^2} - \frac{1}{\lambda_c^2} \right) = - \left[ \frac{1}{2\pi d} \ln \left( \frac{1}{T} \right) \right]^2 \quad (12)$$

Where d is the sample thickness,  $\lambda_o$  is the free space wavelength,  $\lambda_c$  is the cutoff wavelength, the relative the relative permeability of material is given by equation:

$$\mu_r = \frac{1+\Gamma}{\Lambda(1-\Gamma) \left( \frac{1}{\lambda_o^2} - \frac{1}{\lambda_c^2} \right)} \quad (13)$$

The relative permittivity can be described by equation:

$$\epsilon_r = \frac{\left( \frac{1}{\Lambda^2} - \frac{1}{\lambda_c^2} \right) \lambda_o^2}{\mu_r} \quad (14)$$

The reflectivity is calculated for normal incident of electromagnetic wave by using the following equation:

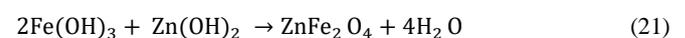
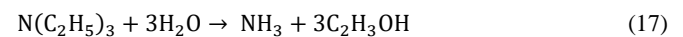
$$R = 20 \log \left| \frac{\sqrt{\frac{\mu_r}{\epsilon_r}} \tanh \left( j \frac{2\pi f}{c} \sqrt{\mu_r \epsilon_r} d \right) - 1}{\sqrt{\frac{\mu_r}{\epsilon_r}} \tanh \left( j \frac{2\pi f}{c} \sqrt{\mu_r \epsilon_r} d \right) + 1} \right| \quad (15)$$

The real part of the propagation constant represents attenuation constant ( $\alpha$ ) and given by:

$$\alpha = \text{Re} \left( \frac{2i \pi f \sqrt{\mu_r \epsilon_r}}{c} \right) = - \frac{\ln|T|}{d} \quad (16)$$

## 3. Experimental

Zinc ferrite fine powders with general formula  $ZnFe_2O_4$  have been prepared by sol-gel method. The raw materials consist of three precursor solution, (0.2M) of  $Fe(NO_3)_3 \cdot 9H_2O$ , (0.2 M) of  $Zn(NO_3)_2 \cdot 6H_2O$ , and (0.2 M) of citric acid  $C_6H_8O_7$  were used in the formation of each sample and separately dissolves in (100 ml) of distilled water. The three solutions are then re-mixed together by continuous stirring by magnetic hot plat. The next concentrations is (0.4M) of iron nitrate, (0.4M) of zinc nitrate also 100 ml of citric acid. The control on pH of the solution was fined at (7.5) by using many drops of ammonia and the solution was heated on the hot plate at 60 °C for 40 min. The temperature of solution increased to 80 °C for (8) hours, the solution was turned into gel. The gel material dried by Leave it several hours, and every gel compounds sintering at (600, 800 and 1000°C) for three hours, for getting a number of samples can by studied before grinding process. The chemical reaction for the formation  $ZnFe_2O_4$  is given when a reaction medium is consisted of a citric acid  $C_6H_8O_7$  and  $NH_3$  in the presence of water under hydrothermal condition. Ammonia reacts with water and forming the alkaline agent, which raise the pH of solution. The alkaline agent leads the formation of  $Zn(OH)_2$  and  $Fe(OH)_3$  the interaction between two compounds through dehydration can be transformed into  $ZnFe_2O_4$  [24].



The fluffy material was ground to get ferrite powder using the Handmade grinder for five minutes, Powders are mixed with glycerin material (7) drop with (7gm) of zinc ferrite powders, The powder was pushed at (3 Tons) by the piston oil to obtain samples as Parallelogram of (23 × 10 × 10) mm in dimensions, where template was used for this purpose, The samples were sintered, for 2 hr. at three sintering temperatures, at (600, 800 and 1000°C). The

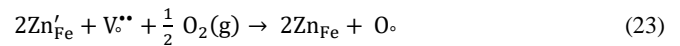
structure and the average crystallite size of the spinal zinc ferrites nanoparticles were examined by X-Ray diffractometer (6000-Shimadzu) by using CuK $\alpha$  ( $\alpha$ ) radiation source with a wavelength,  $\lambda=1.54060$  Å. The morphological and surface distribution of the ZnFe $_2$ O $_4$  particles were analyzed using scanning Probe Microscope (SPM, model AA3000 Angstrom Advanced. Inc). The matrix scattering parameters tests of the Zinc ferrite samples have been carried out for all samples by using the vector network analyzer device type of Anritsu MS4642A (20GHz), in the X-band range (8-12) GHz.

#### 4. Results and discussion

Typical X-ray diffraction pattern has been examined for all samples by X-Ray diffractometer (6000-Shimadzu) with using CuK $\alpha$  ( $\alpha$ ) radiation source in the range (20 to 60 degrees) after sintering at (600, 800 and 1000°C). The diffraction peaks of the pattern is corresponding to the characteristic crystallographic major planes of single phase cubic spinel Zinc Ferrites (220), (311), (222), (400), (422), and (511) are shown in Fig. 1 and Fig. 2. It is clear that all samples had a face-centered cubic crystal structure can be attributed to the spinel ZnFe $_2$ O $_4$  were indexed by comparing with (JCPDS card No. 65-3111). The lattice constant can be measure by using the relation  $a = d(h^2 + k^2 + l^2)^{\frac{1}{2}}$  depending on the most intense peak (3 1 1) and their values varies from ( $a = 8.3781$  Å –  $8.4537$  Å) [13]. Figures shows extra diffraction peaks (\*) belongs to a hematite type of  $\alpha$ -Fe $_2$ O $_3$  nanoparticles are crystallized in hexagonal crystal order with rhombohedral lattice structure. Diffractions peaks orientations of  $\alpha$ -Fe $_2$ O $_3$  nanoparticles in the (113), (024) and (116) major lattice planes which are formed in both molar concentration (0.2 M, 0.4 M), that are excellent corresponding with JCPDS card number 86-0550. A stable phase of  $\alpha$ -Fe $_2$ O $_3$  at sintering temperature (600, 800 and 1000°C) does not react with Zn $^{2+}$  [25]. Also there are diffraction peaks ( $\Delta$ ) that corresponding of orientation (002) and (101) planes that belong to the hexagonal wurtzite structure of ZnO which are in excellent agreement with (JCPDS Card no 36-1451). The high intensity of major diffraction peaks [ $\Delta = (002), \Delta\Delta = (101)$ ] of ZnO which decrease with increasing of the sintering temperature in the molar concentration (0.2M) because of its transformation from ZnO structure to ZnFe $_2$ O $_4$  structure, while structure transformation does not occur in the molar concentration (0.4 M). All peaks of ZnFe $_2$ O $_4$  grow sharply and become high intensity when sintering temperature increased, which mean an improvement of the crystallization of zinc ferrite. The broad diffraction peaks confirm of forming nanoparticles of ZnFe $_2$ O $_4$ . The crystallite size was calculated for the strongest peak broadening (311) plane using Scherrer's equation is given by equation,  $D_{av} = 0.89 \lambda / B \cos \theta$ , where  $\theta$  is the diffraction angle, and B is the full width at half maximum [26]. The sintering process decreases the strain and lattice defects also the crystallite size will be increased when the sintering temperature increased. The structural parameters of the ZnFe $_2$ O $_4$  nanopowder are listed in Table 1. Increase of the particle size for (0.2M) concentration with an increase of the sintering temperature due to increase of zinc ion (Zn $^{2+}$ ) occupancy of the tetrahedral sites, and this leads to migration of iron ions (Fe $^{3+}$ ) and occupancy of the octahedral sites through transformation from a phase of ZnO to ZnFe $_2$ O $_4$  structure. Increasing of zinc ions content in the concentration (0.4M) that is increased the particle size of ZnFe $_2$ O $_4$  structure. It is seen through the table.1, that the lattice constant increase when increase of zinc contents because the radius of zinc ions (0.88 Å) in the tetrahedral site is larger than the(Fe $^{3+}$ ) (0.64 Å) in the octahedral sites, the substitution of (Zn $^{2+}$ ) leads to larger expansion of the lattice constant [27]. Increasing in the lattice constant which occurs when the ZnO is added to the structure, where Zn is replaced for Fe depending on the defect reaction [28].

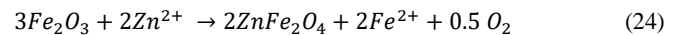


Decreasing in the lattice constant because of the charge compensating oxygen vacancies or the oxidation of Zn $^{2+}$  as in the following interaction:



In addition, there is a decrease in the lattice constant for molar concentration (0.2 M) at 1000 °C may be due to presence of (Zn $^{2+}$ ) ions near the grain boundary. ZnFe $_2$ O $_4$  structure is formed in two ways through two reactions the first reaction at Fe $_2$ O $_3$  - interface through decomposition of Fe $_2$ O $_3$  to 2Fe $^{2+}$  and O $_2$  gas. The second reaction occurs on the ZnO interface by reacting ZnO and Fe $^{2+}$  by addition of oxygen gas.

At Fe $_2$ O $_3$  interface:



At ZnO interface:

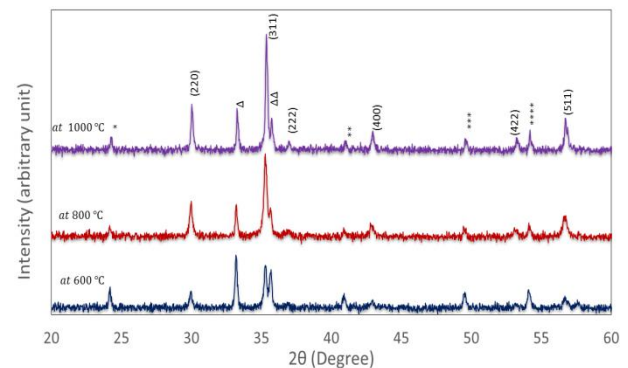
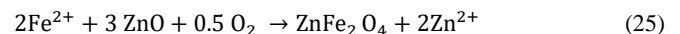


Fig. 1: X-Ray Diffraction Patterns of the Znfe $_2$ o $_4$  Nanoparticles for Molar Concentration (0.2M).

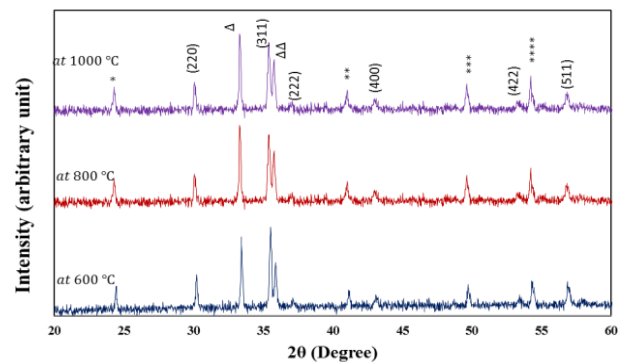


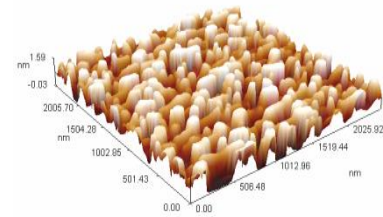
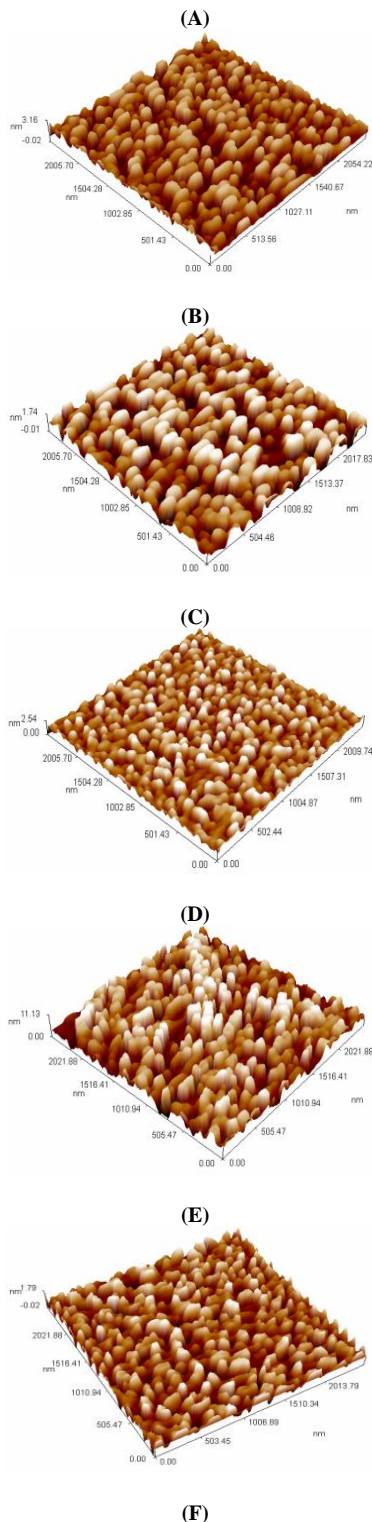
Fig. 2: X-Ray Diffraction Patterns of the Znfe $_2$ o $_4$  Nanoparticles for Molar Concentration (0.4M).

Table 1: The Structural Parameters of the Znfe $_2$ o $_4$  Nanopowder in the (311) Plane.

Molar	Sintering	FWHM (Deg.)	G.S (nm)	$\delta = 1/D^2$	$S = \beta \cos\theta/4$	$d_{hkl}$	Exp. (Å) Lattice
Concentrations	temp(°C)	Constant (Å)					
600	0.27713626	30.114	0.00110265	0.0046099	2.54661564	8.4441	
0.2	800	0.16325635	51.116	0.00038271	0.0027159	2.54898365	8.4537
1000	0.13332564	62.622	0.00025534	0.0022169	2.53695990	8.4139	
600	0.22548209	37.044	0.00072872	0.0037476	2.52617055	8.3781	
0.4	800	0.16038567	52.055	0.00036903	0.0026669	2.53575951	8.4099
1000	0.11528925	72.417	0.00019068	0.0019170	2.53759513	8.4159	

The atomic force microscope was used to examination of the surface morphology of the ZnFe $_2$ O $_4$  nanoparticles samples. Three-dimensional AFM images are appearing the granule structures that have a higher surface area as shown in Fig. 3. And figure showed the uniform distribution of the granules in the form of high lands and valleys with a very smooth surface with small RMS Rough-

ness varies (0.34-0.58 nm) which are summarized in the Table 2. Grain size increases when the temperature of sintering increased from (600 -1000 °C) due to the particles aggregation to form porous structures. Also the grain size is increasing when the molar concentration increases probably due to the large radius of zinc ions than  $Fe^{3+}$ . The importance of the study of surface roughness for materials due to its effect on the optical properties through scattering of light and reduce the reflectivity of electromagnetic waves. The results analysis of Atomic Force Microscopic showed of increasing surface roughness with increased both sintering temperature and molar concentrations. This growth of the surface roughness average is as a result of the grain size increasing.



**Fig. 3:** Atomic Force Microscopy (AFM) Images of ZnFe<sub>2</sub>O<sub>4</sub> Nanoparticles.

**Table 2:** The Average Grain Sizes and Roughness Average of ZnFe<sub>2</sub>O<sub>4</sub> According to Molar Concentrations and Sintering Temperature

Concentration (M)	Temperature (°C)	Avg. Diameter (nm)	Root mean square Roughness Avg. (nm)	Figures
a)	600	70.35	0.413	0.341 Fig. 1.
b)	0.2	800	82.82	0.433 0.39 Fig. 1.
c)	1000	116.60	0.513	0.401 Fig. 1.
d)	600	88.84	0.49	0.414 Fig. 1. (d)
e)	0.4	800	98.67	0.509 0.424 Fig. 1.
f)	1000	118.99	0.678	0.585 Fig. 1.

To determine the scattering matrix elements ( $S_{11}, S_{21}$ ), vector network analyzer were used in the in the X-band range (8-12) GHz. These elements ( $S_{11}, S_{21}$ ) were utilized to calculate the values of ( $\epsilon', \epsilon'', \mu', \mu''$ ) thus can be measured the complex relative permittivity ( $\epsilon_r = \epsilon' - j\epsilon''$ ) and the complex relative permeability ( $\mu_r = \mu' - j\mu''$ ) of materials. The real parts of complex permittivity ( $\epsilon'$ ) and real part of complex permeability ( $\mu'$ ) are represent the storage energy of the electric and magnetic fields. The imaginary parts of complex permittivity ( $\epsilon''$ ) and imaginary part of complex permeability ( $\mu''$ ) are represent the loss of the energy [29]. The values ( $S_{11}, S_{21}$ ) are changing with microwaves frequency, and all the parameters ( $\Gamma^2, A^2, \epsilon_r, \mu_r$ ) will change with frequency because the ferrite materials possess a characteristic of microwaves absorption. The mechanism of absorption in the zinc ferrite material is the domain magnetic wall movement, and rotation of magnetic domain and that depends on the imaginary part of the permeability values and dielectric constant which rely on the internal structure of the ferrite, grain size, sintering temperature, concentrations with secondary phases with the ferrite. The complex relative permeability and permittivity are simulated and calculated by Matlab software using Eqs. (14) and (13). Where the blue color represent the real part of the complex relative permeability and permittivity and the red color represent the imaginary part of the complex relative permeability and permittivity as shown in the Fig. 4 and Fig. 5 respectively. The permeability dispersion with frequency of polycrystalline ferrites materials is affected by two mechanisms the first is domain wall resonance and the second is the spin rotation. The real part of magnetic permeability decreases with increasing frequency for concentrations 0.2M and 0.4M at sintering temperature 600°C because the external field changes rapidly at high frequency, so that the realignment of magnetic dipoles is too difficult with external fields [30]. Real part of magnetic permeability has small and almost constant values with a little fluctuation in the measured frequency range for concentration 0.2M and 0.4M at sintering temperature 800°C and 1000°C. This magnetic parameter decreases gradually with the frequency increase due to the decreasing of both relaxation effects and domain-wall motion. Also substitution of zinc ions (nonmagnetic ion) which occupies A and B sites results in the reduction of the interaction between A and B sites thus changing the magnetic properties of the samples. Increase more in concentration of zinc ions leads to decrease of saturation magnetization, as well as increase in zinc concentration may be causes to the decrease in anisotropy field, which reduces the domain wall energy [31]. The imaginary part of the permeability or (magnetic loss) generated from the magnetic damping resulting from ferromagnetic resonance and domain wall motion. The imaginary part of magnetic permeability as shown in Fig. 4 is approaching zero with negative values at certain frequencies. Magnetic losses defined by the imaginary part of permeabil-

ity and mainly occur because domain wall resonance in the material, eddy current loss, neutral resonance, magnetic hysteresis and exchange resonance [32]. High resistivity of ferrite materials causes a low magnetic loss and this is because the resistivity is inversely proportional to the eddy currents. The negative value of imaginary part of permeability is found to be coupled with positive maxima of imaginary part of permittivity due to a phase lag between inductance and capacitance in the system [33]. The negative imaginary parts of permeability have been observed in many nanocomposite systems within the high frequency range, such as multiwalled carbon nanotube, hollow cobalt nanochains, and SiC nanowire. There are four types of polarization is contributed in dielectric constant at lower frequency (ionic, electronic, orientation and space charge polarization), but at high frequencies some types of polarization do not contribute in the dielectric constant which leads to reduce in the dielectric constant  $\epsilon_r$ . At lower frequencies the electrons hopping between ions  $\text{Fe}^{+3}$  and  $\text{Fe}^{+2}$  at octahedral sites have higher frequency as compared to the frequency of AC applied field so the interaction is easy with the applied field causing an increase in the dielectric constant. Low values of the dielectric constant at high frequencies due to frequency of hopping electrons cannot follow the frequency of applied field and the electron exchange is perturbed between  $\text{Fe}^{+2}$  and  $\text{Fe}^{+3}$  [34]. The dielectric properties of polycrystalline ferrite materials arise from the intrinsic electric dipole polarization and the interfacial polarization. The real and imaginary parts of the permittivity remains nearly constant and low values with increasing frequency for concentrations 0.2M and 0.4M at sintering temperature 600°C, there are also some fluctuations in values for two parts of permittivity for concentration 0.2M and 0.4M at sintering temperature 800°C and 1000°C as shown in Fig. 5. The constant values for real part of permittivity means there was a dominant one type of polarization, which the oscillation of the dipole moments was in phase or out of phase with the microwave frequency. Dielectric constant (real part) decreases with increase the frequency because the dipoles in the ferrites materials cannot reorient themselves along the applied field. The dielectric loss is expressed by imaginary part of permittivity that generated from damping of the vibrating dipole moments and conductor loss. The low values of imaginary part of permittivity (dielectric loss) may be due to decrease of dipole polarization that is contributed to the dielectric dissipation factors. Also the change in the particle size and parameters leads to increase of the complex permittivity and complex permeability. Magnetic losses are more important and effective for microwave absorption than dielectric losses. Reflectivity and absorbance of the ferrite materials depends on the microwaves frequency as shown in the Fig. 6 (blue color represents the reflectivity  $\Gamma^2$  and red color represents absorbance  $A^2$ ). The best desired absorbance of microwave waves can be achieved at the low values of the sintering temperature (600°C) for two concentration where the reflectivity of the waves at the minimum value. The weak absorption of the microwave when using an excessive amount of the zinc oxide concentration at sintering temperature (800°C and 1000°C) due to increase the electric resistivity of the ferrite material through growing of electron scattering which leads to increase defects, there is also an increase in ohmic loss and the microwave absorption is not conducive to impedance matching [35]. Increase the absorption of two concentrations at the sintering temperature (600°C) that leads to more attenuation of the electromagnetic waves, which they attribute to existence of magnetic materials and high dielectric constant materials that increase more the scattering of the wave inside the material. It is also possible to observe attenuation phenomena at certain frequencies of other samples at sintering (800 and 1000°C) as shown in Fig. 7.

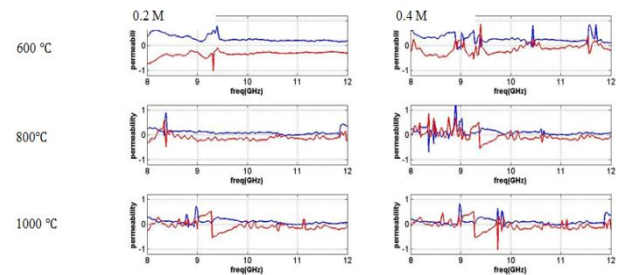


**Fig. 4:** The Relative Permeability (Blue Color Is the Real Part, Red Color Is Imaginary Part) as A Function of the Frequency at Three Different Temperatures for (0.2 M) and (0.4 M) Concentrations.

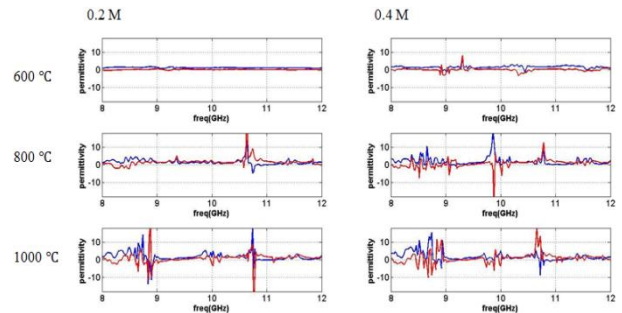


**Fig. 5:** The Relative Permittivity (Blue Color Is the Real Part, Red Color Is Imaginary Part) as A Function to the Frequency at Three Different Temperatures for (0.2 M) and (0.4 M) Concentrations.

Enhancement the microwaves absorbing of the ferrite materials by substitution that making the smaller crystallite size and deformed the lattice constant which increases the repeated reflection of microwaves inside the ferrite material that leads for more energy be absorbed. Also the substitution influence on the absorption coefficient and the attenuation of microwave by increasing in values of the imaginary part of permeability and imaginary part of permittivity [36].

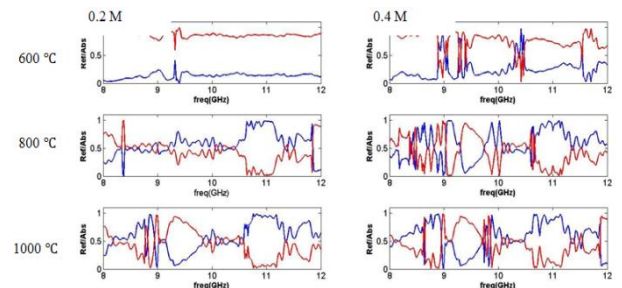


**Fig. 6:** The Reflection (Blue Color), Absorbance (Red Color) as A Function to the Frequency at Three Different Temperatures for (0.2 M) and (0.4 M) Concentrations.

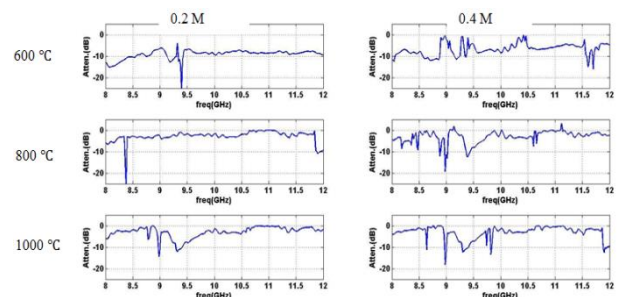


**Fig. 7:** The Attenuation Coefficient as A Function to the Frequency at Three Different Temperatures for (0.2 M) and (0.4 M) Concentrations.

## 5. Conclusions

$\text{ZnFe}_2\text{O}_4$  nanoparticles have been prepared successfully by using Sol-Gel method at difference temperature. Different phases from hematite type of  $\alpha\text{-Fe}_2\text{O}_3$  and the hexagonal wurtzite structure of ZnO were observed in addition to zinc ferrites structure due to use

a high concentration of  $\text{Zn}(\text{NO}_3)_2 \cdot 6\text{H}_2\text{O}$ . Complex permeability measurements revealed low values of the real part of permeability due to the decreasing of both relaxation effects and domain-wall motion. The imaginary part of permeability is approaching zero with negative values at certain frequencies because high resistivity of ferrite materials causes a low magnetic loss. The real and imaginary parts of the permittivity remains nearly constant with low values with increasing frequency for concentrations 0.2M and 0.4M at sintering temperature 600°C. The constant values for real part of permittivity means there was a dominant one type of polarization, which the oscillation of the dipole moments was in phase or out of phase with the microwave frequency. The best desired absorbance of microwave waves can be achieved at the sintering temperature (600°C) for two concentrations that leads to more attenuation of the electromagnetic waves.

## Acknowledgements

The authors gratefully extend thanks to the university of wasit - college of science.

## References

- Y. Liu, S. C. Wei, Y. J. Wang, H. L. Tian, H. Tong, and B. S. Xu, "Characterization of (Mg, La) substituted Ni-Zn Spinel Ferrite", *Physics Procedia*, vol. 50, pp. 43-47, 2013. <https://doi.org/10.1016/j.phpro.2013.11.009>.
- Y. Hwang, "Microwave Absorbing Properties of NiZn-Ferrite synthesized from Waste Iron Oxide Catalyst", *Materials letters*, vol. 60, pp. 3277-3280, 2006. <https://doi.org/10.1016/j.matlet.2006.03.010>.
- L. H. Gul, W. Ahmed, A. Maqsood, "Electrical and Magnetic Characterization of Nanocrystalline Ni-Zn Ferrite Synthesis by Co-Precipitation Route", *Journal of Magnetism and Magnetic Materials*, vol. 320, pp. 270-275, 2008. <https://doi.org/10.1016/j.jmmm.2007.05.032>.
- L. D. Tung, V. Kolesnichenko, G. Caruntu, D. Caruntu, Y. Remond, V. O. Golub, C. J. O. Connor, L. Spinu, "Annealing effects on the Magnetic properties of nanocrystalline Zinc Ferrite", *Physica B: Condensed Matter*, vol. 319, pp. 116-121, 2002. [https://doi.org/10.1016/S0921-4526\(02\)01114-6](https://doi.org/10.1016/S0921-4526(02)01114-6).
- I. V. Kasiviswanath, Y. L. N. Murthy, K. Tata, R. Singh, "Synthesis and Characterize of nano Ferrites by Citrate Gel Methods", *International Journal of Chemical Sciences*, vol. 11, pp. 64-72, 2013. <http://www.tsijournals.com/articles/synthesis-and-characterization-of-nanoferrites-by-citrate-gel-method.pdf>.
- L. Gunther, "Quantum tunneling of magnetization", *Physics World*, vol. 3, pp. 28, 1990. <https://doi.org/10.1088/2058-7058/3/12/21>.
- I. Zalite, G. Heidemane, A. Krumina, D. Rasmene, M. Maiorov, "ZnFe<sub>2</sub>O<sub>4</sub> Containing Nanoparticles: Synthesis and Magnetic Properties", *Materials Sciences & Applied Chemistry*, vol. 34, pp. 38-44, 2017. <https://doi.org/10.1515/msac-2017-0006>.
- A. C. F. M. Costa, E. Tortella, M. R. Morelli, R. H. A. Kiminami, "Synthesis, microstructure and magnetic properties of Ni-Zn ferrites", *Journal of Magnetism and magnetic Materials*, vol. 256, pp. 174-182, 2003. [https://doi.org/10.1016/S0304-8853\(02\)00449-3](https://doi.org/10.1016/S0304-8853(02)00449-3).
- P. Priyadharsini, A. Pradeep, G. Chandrasekaran, "Novel combustion route of synthesis and characterization of nanocrystalline mixed ferrites of Ni-Zn", *Journal of Magnetism and magnetic Materials*, vol. 321, pp. 1898-1903, 2009. <https://doi.org/10.1016/j.jmmm.2008.12.005>.
- H. Sharma, S. Jain, P. M. Raj, K. P. Murali, R. Tummala, "Magnetic and Dielectric Property Studies in Fe- and NiFe-Based Polymer Nanocomposites", *Journal of Electronic Materials*, vol. 44, pp. 3819-3826, 2015. <https://doi.org/10.1007/s11664-015-3801-x>.
- T. A. S. Ferreira, J. C. Waerenborgh, M. H. R. M. Mendonca, M. R. Nunes, F. M. Coasta, "Structural and morphological characterization of FeCo<sub>2</sub>O<sub>4</sub> and CoFe<sub>2</sub>O<sub>4</sub> spinels prepared by a coprecipitation method", *Solid State Science*, vol. 5, pp. 383-392, 2003. [https://doi.org/10.1016/S1293-2558\(03\)00011-6](https://doi.org/10.1016/S1293-2558(03)00011-6).
- N. Millot, S. LeGallet, D. Aymes, F. Bemard, Y. Grin, "Spark plasma sintering of cobalt ferrite nanopowders prepared by coprecipitation and hydrothermal synthesis", *Journal of the European Ceramic Society*, vol. 27, pp. 921-926, 2007. <https://doi.org/10.1016/j.jeurceramsoc.2006.04.139>.
- S. I. Abbas, H. T. John, A. J. Fraih, "Preparation of Nano Crystalline Zinc -Ferrite as Material for Micro Waves Absorption by Sol-Gel Methods", *Indian Journal of Sciences & Technology*, vol. 10, 2017. <https://doi.org/10.17485/ijst/2017/v10i21/113197>.
- C. G. Anchieta, A. Cancelier, M. A. Mazutti, S. L. Jahn, R. C. Kuhn, A. Gundel, O. C. Filho, E. L. Foltto, "Effects of Solvent Diols on the Synthesis of ZnFe<sub>2</sub>O<sub>4</sub> Particles and Their Use as Heterogeneous Photo-Fenton", *Catalysts Materials*, vol. 7, pp. 6281-6290, 2017. <https://doi.org/10.3390/ma7096281>.
- C. B. R. Jesus, E. C. Mendonca, L. S. Silva, W. S. D. Folly, C. T. Meneses, J. G. S. Duque, "Weak ferromagnetic component on the bulk ZnFe<sub>2</sub>O<sub>4</sub> compound", *Journal of Magnetism & Magnetic Materials*, vol. 350, pp. 47-49, 2014. <https://doi.org/10.1016/j.jmmm.2013.09.025>.
- I. Mohai, J. Szépvölgyi, I. Bertóti, M. Mohai, J. Gubicza, T. Ungár, "Thermal plasma synthesis of zinc ferrite nanopowder", *Solid State Ion*, Vol. 141, pp. 163-168, 2001. [https://doi.org/10.1016/S0167-2738\(01\)00770-6](https://doi.org/10.1016/S0167-2738(01)00770-6).
- A. Simona, P. Vlazan, S. Novaconi, I. Grozescu, P. V. Notingher, "Electromagnetic behavior of zinc ferrites obtained by a coprecipitation technique", *U. P. B. Sci. Bull., Series C*, vol. 73, 2011. <https://www.researchgate.net/publication/265523408>.
- W. W. Jie, Z. C. Guang, J. Q. Jie, "Fabrication and performance optimization of Mn-Zn ferrite/EP composites as microwave absorbing materials", *Chin. Phys. B*, vol. 22, 2013. <https://doi.org/10.1088/1674-1056/22/12/128101>.
- V. Y. Liao, "Modern Microwave Technology", Ellis Horwood Limited, New York, 1987.
- L. F. Chen, C. Ong, C. Neo, "Microwave Electronics Measurement and Materials Characterization", John Wiley & Sons, 2004. <https://onlinelibrary.wiley.com/doi/book/10.1002/0470020466>. <https://doi.org/10.1002/0470020466>.
- H. Bayrakdar, "Electromagnetic propagation and Absorbing property of Ferrite-Polymer Nanocomposite structure", *Progress in Electromagnetic Research M*, vol. 25, pp. 269-281, 2012. <https://doi.org/10.2528/PIERM12072303>.
- A. B. Nicolson, G. F. Ross, "Measurement of the intrinsic properties of materials by time-domain techniques", *IEEE Transaction on Instrumentation & Measurement IM*, vol. 19, pp. 377-382, 1970. <https://doi.org/10.1109/TIM.1970.4313932>.
- A. L. De paula, M. C. Rezende, J. J. Barroso, "Experimental measurements and numerical simulation of permittivity and permeability of Teflon in X band", *Journal Aerospace Technology & Management*, vol. 3, pp. 59-64, 2011. <https://doi.org/10.5028/jatm.2011.03019410>.
- Z. Z. Lazarevic, C. Jovalekic, V. N. Ivanovski, A. Recnik, A. N. Milutinovic, B. Cekic, N. Z. Romcevic, "Characterization of partially inverse spinel ZnFe<sub>2</sub>O<sub>4</sub> with high saturation magnetization synthesized via soft mechanochemically assisted route", *Journal of physics and chemistry of solids*, vol. 75, pp. 869-877, 2014. <https://doi.org/10.1016/j.jpcs.2014.03.004>.
- G. Z. Shen, G. S. Cheng, Y. Cao, Z. Xu, "Preparation and microwave absorption of M type ferrite nanoparticle composites", *Materials Science - Poland*, vol. 28, pp. 327-334, 2010. [http://www.materialscience.pwr.wroc.pl/bi/vol28no1/articles/ms\\_3\\_2\\_2009\\_114shen.pdf](http://www.materialscience.pwr.wroc.pl/bi/vol28no1/articles/ms_3_2_2009_114shen.pdf).
- S. E. Jacobo, J. C. Apesteguy, N. N. Shegoleva, G. V. Kurylanskaya, "Structural and Magnetic Properties of Nanoparticles of NiCuZn Ferrite Prepared by the Self-Combustion Method", *Solid State Phenomena*, vol. 168, pp. 333-340, 2011. <https://doi.org/10.4028/www.scientific.net/SSP.168-169.333>.
- A. Khan, M. A. Bhuiyan, G. Al-Quaderi, K. H. Maria, S. Choudhury, K. A. Hossaini, S. Aktheri, D. K. Saha, "Dielectric and Transport Properties of Zn-Substitute Cobalt Ferrites", *Journal Bangladesh Academy of Sciences*, vol. 37, pp. 73-82, 2013. <https://doi.org/10.3329/jbas.v37i1.15683>.
- H. Vu, D. Nguyen, J. G. Fisher, W. Hamoon, S. Bae, H. G. Park, B. G. Park, "CuO - based sintering aids for low temperature sintering of BaFe<sub>12</sub>O<sub>19</sub> ceramics", *Journal of Asian Ceramic Societies*, vol. 1, pp. 170-177, 2013. <https://doi.org/10.1016/j.jascers.2013.05.002>.
- A. Kumar, V. Agarwala, D. Singh, "Effect of particles size of BaFe<sub>12</sub>O<sub>19</sub> on the Microwave absorption characteristic in X-band", *Progress International Electromagnetics Research M*, vol. 29, pp. 223-236, 2013. <https://doi.org/10.2528/PIERM13011604>.
- A. Mandal, D. Ghosh, A. Malas, P. Pal, C. K. Das, "Synthesis and Microwave Absorbing properties of Cu-Doped Nickel Zinc Ferrite/Pb (Zr<sub>0.52</sub> Ti<sub>0.48</sub>) O<sub>3</sub> nanocomposites", *Journal of Engineering*, 2013. <https://doi.org/10.1155/2013/391083>.
- S. Singhal, T. Namgyal, S. Bansal, K. Chandra, "Effect of Zn Substitution on the Magnetic properties of Cobalt Ferrite Nanoparticles Prepared Via Sol-Gel Route", *Journal Electromagnetic Analysis*

- &Application, vol.2, pp. 376-381, 2010. <https://doi.org/10.4236/jemaa.2010.26049>.
- [32] S. K. Dhawan, A. Ohlan, K. Dingh, "Designing of Nano Composites of Conducting Polymers for EMI Shielding, Advances in Nanocomposites - Synthesis Advances in Nanocomposites – Synthesis", Characterization and Industrial Applications, pp. 430-481, 2011. <https://doi.org/10.5772/14752>.
- [33] D. Li, Y. Feng, D. S. Pan, L. W. Jiang, Z. M. Dai, S. J. Li, Y. Wang, J. He, W. Liu, Z. D. Zhang, "Negative Imaginary Parts of Complex Permeability and Microwaves Absorption Performance of Core double –Shelled FeCo/C/ Fe<sub>2.5</sub>Cr<sub>0.5</sub>Se<sub>4</sub> Nanocomposites", Royal Society of Chemistry, vol.6, pp.73020-73027,2016. <https://doi.org/10.1039/C6RA12772J>.
- [34] U. N. Trivedi, M. C. Chhantbar, K. B. Modi, H. H. Joshi, "Frequency dependent dielectric behavior of Cadmium and Chromium Co- substituted nickel ferrite," Indian Journal of Pure & Applied Physics, vol. 43, pp. 688-690, 2005. <https://pdfs.semanticscholar.org/3c4d/b73d3016cccf4e36194c5b497701b5b673d1.pdf>.
- [35] X. Qin, Y. Cheng, K. Zhou, S. Huang, X. Hui, "Microwave Absorbing Properties of W-Type Hexa ferrite Ba(MnZn)<sub>x</sub>Co<sub>2(1-x)</sub>Fe<sub>16</sub>O<sub>27</sub>", Journal of Materials Science and Chemical Engineering, vol. 1, pp. 8-13, 2013. <https://doi.org/10.4236/msce.2013.14002>.
- [36] N. Chen, M. Gu, "Microstructure and Microwave Absorption Properties of Y- Substituted Ni-Zn Ferrites", Open Journal of Metal, vol. 2, pp.37- 41, 2012. <https://doi.org/10.4236/ojmetal.2012.22006>.